*Italian Journal of Food Science, 2021; 33 (3): 1–13*

# Formulation and optimization of astaxanthin nanoemulsions with marine phospholipids derived from large yellow croaker (*Larimichthys crocea*) roe

**Luyao Huang[a,b], Lingyun Zhang[b], Ruifen Li[c], Peng Liang[a,b,*]**

*[a]Engineering Research Centre of Fujian-Taiwan, Special Marine Food Processing and Nutrition, Ministry of Education, Fuzhou 350002, PR China; [b]College of Food Science, Fujian Agriculture and Forestry University, Fuzhou 350002, PR China; [c]Section for Ingredients and Dairy Technology, Department of Food Science, University of Copenhagen, Rolighedsvej 26, DK-1958 Frederiksberg C, Denmark*

***Corresponding Authors:** Peng Liang, Engineering Research Centre of Fujian-Taiwan, Special Marine Food Processing and Nutrition, Ministry of Education, Fuzhou 350002, PR China. Email: liangpeng137@sina.com

Received: 3 March 2021; Accepted: 2 August 2021; Published: 9 September 2021


**PAPER**

## Abstract

The aim of this work was to investigate the emulsifying capacity of marine phospholipids derived from large yellow croaker roe (LYCRPLs). Initially, conditions for preparing astaxanthin (1% w/w) nanoemulsions with LYCRPLs were optimized based on single-factor experiments, including homogenization pressure, homogenization cycle, emulsifier concentration and corn oil concentration via the response surface methodology. The optimal homogenization pressure was 60 MPa, the optimal number of homogenization cycles was nine, the optimal emulsifier concentration was 4.7%, and the optimal oil concentration was 20%. Under these conditions, the stability, particle size and polydispersity index of nanoemulsions were 0.018 ± 0.0016, 247 ± 4.5 nm and 0.215±0.019, respectively. The droplets of nanoemulsions were characterized by transmission electron microscopy, which revealed that all the droplets were more or less spherical and nonaggregated. In addition, the storage experiments indicated that the nanoemulsions were stable at different temperatures. Therefore, LYCRPLs could be explored as carriers for the delivery of insoluble bioactive compounds in the food industry.

*Keywords:* astaxanthin, emulsifier, large yellow croaker roe, nanoemulsions, phospholipids

## Introduction

An emulsifier is a substance that improves surface tension between various constituent phases in an emulsion and make them form a uniform and stable dispersion system or emulsion (Dickinson, 2009). Depending on the source, two types of emulsifiers exist: natural and synthetic. In recent years, natural emulsifiers have aroused great interest in food and other industries due to their safety, nutritiousness and other advantages, and they have been gradually replacing synthetic emulsifiers (Kim *et al*., 2020). At present, the commonly used food emulsifiers are proteins, polysaccharides, phospholipids and other surfactants (Kralova and Sjöblom, 2009; Xi *et al*., 2018). Many studies have shown that phospholipids possess a significant capacity to serve as emulsifiers. For example, Komaiko *et al*. (2016) found that sunflower phospholipids were an effective natural emulsifier to transport ω-3 polyunsaturated fatty acids to food products. Donsì *et al*. (2011) successfully prepared the emulsion using soybean lecithin. In addition, McClements and Gumus (2016) compared the effects of different natural emulsifiers (soybean lecithin, whey protein and Arabic gum) for preparing corn oil-in-water nanoemulsions. The results showed that phospholipids have good emulsifying capacity.

Large yellow croaker (*Larimichthys crocea*) is one of the major economic marine fish in China, and it is mainly found distributed in Fujian Province. It has been widely consumed due to its delicious taste and nutrition value

(Hui *et al*., 2016). Large yellow croaker roe is a major by-product obtained during the processing of large yellow croaker, which has the advantages of low pricing and easy availability of raw materials. In our previous study (Liang *et al*., 2018), we found that large yellow croaker roe contains large amount of marine phospholipids (MPLs), and their phospholipid species and molecular types have been determined carefully. Recently, MPLs have become the focus of further research. MPLs predominantly contain docosahexaenoic acid (DHA) or eicosa pentaenoic acid (EPA) (Liang *et al*., 2018). However, no findings have been reported on the emulsification capacity of MPLs derived from large yellow croaker roe. Therefore, we assume that large yellow croaker roe phospholipids (LYCRPLs) can be explored as carriers for the delivery of insoluble bioactive compounds in the food industry.

Astaxanthin (AST) is a carotenoid pigment found in numerous organisms (Pan-Utai *et al*., 2021). It is known for its impact on physiological functions, which include anti-oxidative (Pogorzelska *et al*., 2017), anti-tumor (Nagendraprabhu and Sudhandiran, 2011), and anti-inflammatory properties (Ju *et al*., 2017) as well as its ability to improve vision (Li *et al*., 2012), etc. Consequently, AST has the potential for a broad range of applications in functional foods. However, AST is a hydrophobic substance, and its utilization in the food is limited due to its insolubility (Ambati *et al*., 2014). Numerous studies have shown that nanoemulsion technology is an effective method for carrying AST, which can improve its water solubility and bioavailability (Martínez-Delgado *et al*., 2017; Liu *et al.,* 2019). Therefore, we assume that LYCRPLs may emulsify and improve the solubility of AST. Meanwhile, new and more effective means are required to make high-value use of large yellow croaker roe.

The present study aimed to formulate and optimize AST nanoemulsions to prepare AST nanoemulsions with MPL derived from large yellow croaker roe effectively. Homogenization pressure, homogenization cycles, emulsifier concentration and oil concentration were optimized systematically based on the response surface methodology (RSM) for preparing nanoemulsions, and the same were characterized by transmission electron microscopy (TEM). Furthermore, particle size, polydispersity index (PDI) and zeta-potential of nanoemulsions were measured during the 28-day storage period.

## Materials and Methods

### Materials

Large yellow croaker roe phospholipids containing 76.36% phosphatidylcholine, 12.30% lysophosphatidylcholine, 9.12% phosphatidylethanolamine, 1.09% phosphatidylinositol and 98.87% total phospholipids were obtained from the aquatic food products lab in Fujian Agriculture and Forestry University and prepared and characterized. AST (≥97%) was purchased from Sigma-Aldrich (St. Louis, MO, USA). Refined corn oil was purchased from the local supermarket (Fuzhou City, Fujian Province). All chemicals were obtained from Sinopharm Chemical Reagent Co. Ltd (Fujian, China). Double-distilled water (Milli-Q) was used to prepare all solutions and nanoemulsions.

### Preparation of nanoemulsions

The nanoemulsions were prepared according to the method provided by Shu *et al.* (2018) with some modifications. An oil phase was prepared by dissolving 1% (w/w) AST in refined corn oil (Figure 1). The mixtures were stirred for 2 h at ambient temperature and subsequently filtered through a 0.45-μm membrane. The aqueous phase was prepared by dispersing LYCRPLs in Milli-Q water. Three homogenization steps were performed to formulate AST nanoemulsions. First, coarse emulsions containing 5–25% (w/w) oil phase and 95– 75% (w/w) aqueous phase were stirred constantly using a magnetic stirrer for 2 h. Next, coarse emulsions were treated via a handheld homogenizer (HN-3K, Hanuo, Shanghai, China) at 20,000 rpm for 5 min. In the last step, the resulting coarse emulsions were passed through an ultra-high-pressure nano-homogenizer (FB-110Q, Litu, Shanghai, China) for 1–7 cycles at a homogenization pressure of 10–80 MPa at ambient temperature. All operating conditions were studied at different levels. The obtained nanoemulsions were stored at 4°C prior to further analysis.

### Measurement of particle size, polydispersity index and zeta-potential

The particle size, PDI and zeta-potential of nanoemulsions were measured by dynamic light scattering using a Zeta sizer Nano-ZS90 (Malvern Instruments, Worcestershire, UK). This instrument is able to measure particle sizes ranging from 0.3 to 5,000 nm. The refractive indices of both aqueous and oil phases were set at 1.333 and 1.476, respectively. The samples for measurement were diluted with Milli-Q water at a ratio of 1:500 (v/v) and then placed in the measurement cell. The particle size of nanoemulsions was expressed as *z*-average diameter.

### Measurement of stability of nanoemulsions

The stability of nanoemulsions was determined using a stability analyzer LUMFuge (LUMiFuge111, Berlin,

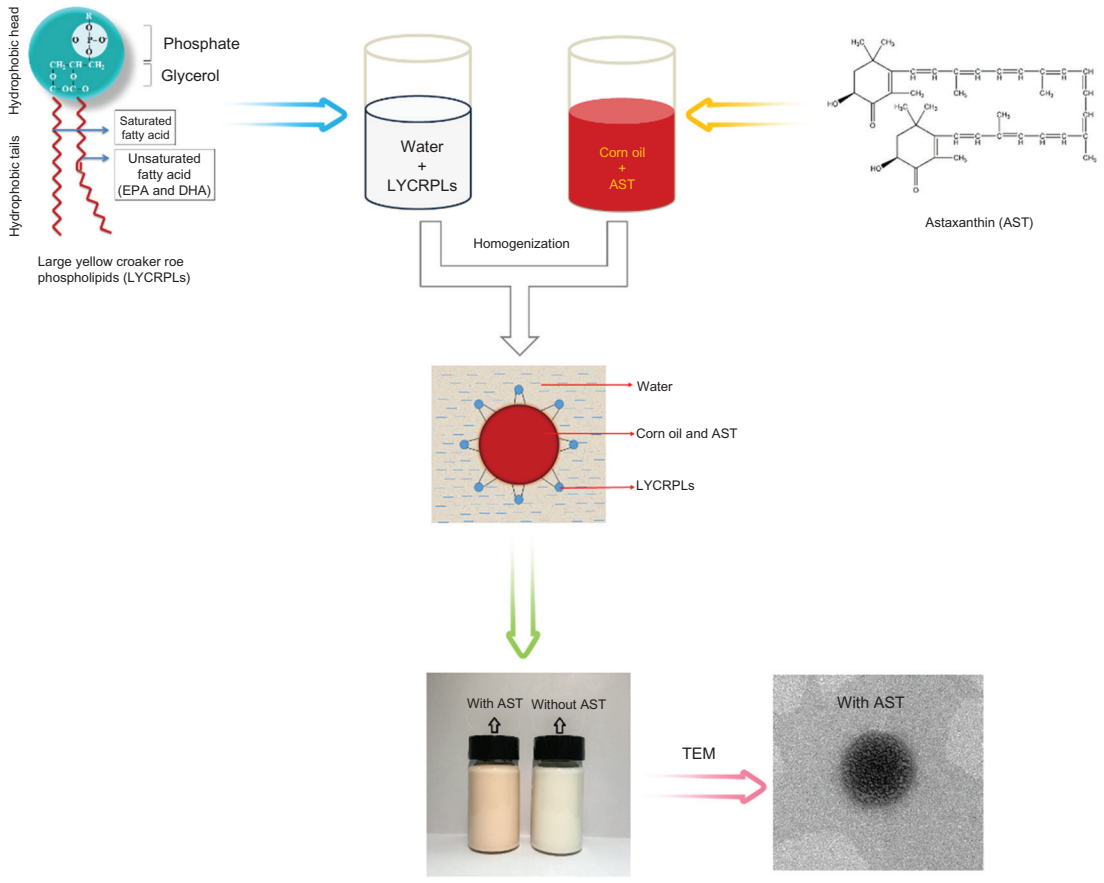


**Figure 1. Schematic diagram of preparation of AST nanoemulsions stabilized by LYCRPLs.**

Germany). The centrifuge quantifies the stability of the dispersion system by continuously recording dynamic changes in the light transmittance of samples. First, 470-mL nanoemulsion is added in the centrifuge tube, and the tube is subsequently placed in the LUMiFuge111. The operating conditions were 3,000 rpm for 10 min at 20°C. The computer automatically records the light transmittance spectra of the sample.

## Microscopic observation of nanoemulsions

The microscopic observation was carried out by using a transmission electron microscope (TEM, HT770, Hitachi Corporation, Japan). Prior to observation by TEM, the nanoemulsions were diluted to acertain concentration with double-distilled water. The appropriate amount of emulsion is absorbed and dripped onto a copper mesh covered with a carbon film. After waiting for 1 min, the remaining liquid was dried using a filter paper. The particles were stained for 1 min with 1% phosphotungstate. The excessive liquid was absorbed by the filter paper and dried naturally, and morphology of the particles was observed by TEM (80 kV).

## Experimental design

### *Single-factor experiments*

Single-factor experiments were applied to determine the appropriate range of variables before response surface optimization. Four independent variables were examined in different ranges (Table 1): 10–80 MPa homogenization pressure, 1–7 cycles in a homogenizer, 2–5% concentration of emulsifier, and 5–25% oil concentration. In addition, effects of variables on the particle size and stability of nanoemulsions were determined as described in Sections 2.4 and 2.5.

### *Response surface experiments*

Central Composite Design (CCD) was selected as the experimental RSM design for optimizing AST

**Table 1. Processing variables used to run experiments.**

| Processing variables | Levels | | | | |
|---|---|---|---|---|---|
| Homogenization pressure (MPa) | 10 | 20 | 40 | 60 | 80 |
| Homogenization cycles | 1 | 2 | 3 | 5 | 7 |
| Emulsifier concentration (%) | 2.0 | 2.5 | 3.0 | 4.0 | 5.0 |
| Oil concentration (%) | 5 | 10 | 15 | 20 | 25 |

nanoemulsion formulations. The experimental ranges, −α, −1, 0, +1 and +α, were chosen taking into account the results obtained from single-factor experiments, which are summarized in Table 2. The response variables were stability, particle size and PDI of nanoemulsions. All experiments were executed in a random order. The relationship between coded and uncoded values is given by Equation (1):

$$Y_0 = \frac{(y_0 - y)}{\Delta y_0}, \quad (1)$$

where $Y_0$ and $y_0$ represent coded and actual values of independent variables, respectively. $\Delta y_0$ indicates step change whereas '$y$' is the central value. Specific equations for homogenization pressure ($X_1$), homogenization cycles ($X_2$), emulsifier concentration ($X_3$), and oil concentration ($X_4$) are as follows:

$$y = \frac{P - 600}{100(2)} \; y_2 = \frac{C - 7}{1}, \quad (2)$$

$$y_3 = \frac{E - 4}{0.5}, \quad (3)$$

$$y_4 = \frac{O - 5}{2.5}, \quad (4)$$

where $P$, $C$, $E$, and $O$ represent homogenization pressure (MPa), homogenization cycles, emulsifier concentration (%), and oil concentration (%), respectively.

A second-order polynomial equation was used to express the stability ($Y_1$), particle size ($Y_2$) and PDI ($Y_3$) of nanoemulsions as a function of independent variables as follows:

$$\begin{aligned} Y_i = {} & \beta_0 + \beta_1 X_1 + \beta_2 X_2 + \beta_3 X_3 + \beta_4 X_4 + \beta_{11} X_{21} \\ & + \beta_{22} X_{22} + \beta_{33} X_{23} + \beta_{44} X_{24} + \beta_{12} X_1 X_2 \\ & + \beta_{13} X_1 X_3 + \beta_{14} X_1 X_4 + \beta_{23} X_2 X_3 + \beta_{24} X_2 X_4 \\ & + \beta_{34} X_3 X_4, \end{aligned} \quad (5)$$

where $Y_i$ represents the response values, $\beta_0$ is a constant, and $\beta_i$, $\beta_{ii}$, and $\beta_{ij}$ indicate the linear, quadratic, and interactive coefficients, respectively. The coefficients of the equation were determined using Design expert software version 10.0.7.

### Storage stability of nanoemulsions

The LYCRPLs–AST nanoemulsions were prepared according to the optimal conditions obtained from the response surface optimization experiments. The storage temperature was controlled at 5°C, 25°C and 55°C for 28 days. Particle size, PDI and zeta-potential of nanoemulsions were measured at scheduled periods (every 7 days). The methods for determination of particle size, PDI and zeta-potential are described in Section 2.4.

### Statistical analysis

The experimental data were analyzed by multiple regression to fit the second-order polynomial equation for independent variables. The significant differences between these independent variables were tested by analysis of variance (ANOVA). The contour plots and response surface plots were created using Design expert software (version 10.0.7) to visualize the influence of independent variables on response variables. Each experiment was performed in triplicate.

## Results and Discussion

### Single-factor experiments

The effects of homogenization pressure on the particle size and stability of nanoemulsions are shown in Figures 2A and 3A. The particle size of nanoemulsions decreased as the homogenization pressure increased, which is consistent with the stability results. A possible explanation could be that increasing the homogenization pressure results in enhancement of shear force and action strength, which makes nanoemulsions more uniform (Floury *et al.*, 2003). However, the internal temperature of the instrument increases when in operation as the homogenization pressure increases (when

**Table 2. Coded and uncoded independent variables used in response surface methodology design.**

| Independent variable | Symbol | Coded levels | | | | |
|---|---|---|---|---|---|---|
| | | −α | −1 | 0 | +1 | +α |
| Homogenization pressure (MPa) | $X_1$ | 40 | 50 | 60 | 70 | 80 |
| Homogenization cycles | $X_2$ | 5 | 6 | 7 | 8 | 9 |
| Emulsifier concentration (%) | $X_3$ | 3.0 | 3.5 | 4.0 | 4.5 | 5.0 |
| Oil concentration (%) | $X_4$ | 10.0 | 12.5 | 15.0 | 17.5 | 20.0 |

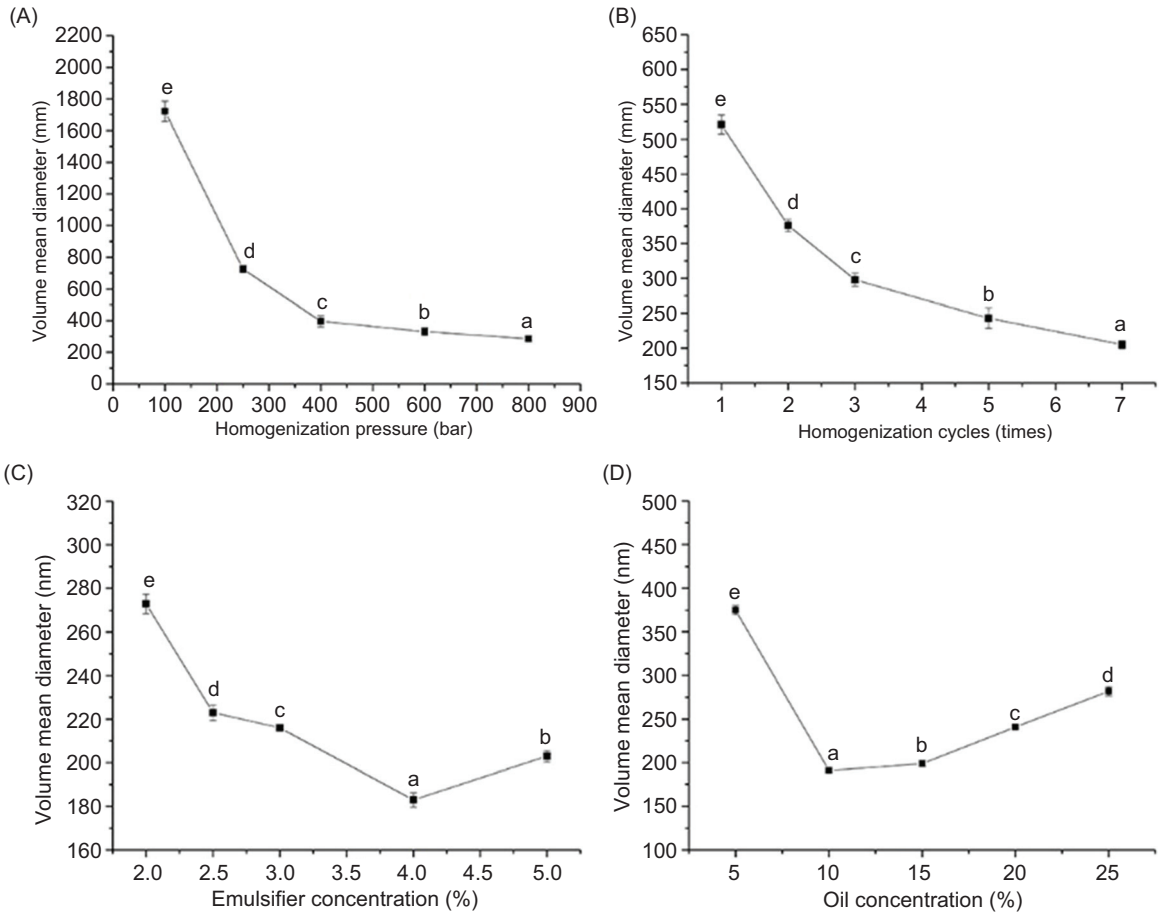


**Figure 2. Effects of (A) homogenization pressure, (B) homogenization cycles, (C) emulsifier concentration and (D) oil concentration on the particle size of AST nanoemulsions.**

the pressure is higher than 60 MPa), which might result in the deterioration of nanoemulsions. Therefore, a homogenization pressure of 60 MPa was selected as the central point to carry out the response surface optimization test. The fixed variables were five homogenization cycles, 3.0% emulsifier concentration and 10% oil concentration.

Nanoemulsions display lower particle size and better stability as the number of homogenization cycles increases (Figures 2B and 3B), which agrees with the effects of homogenization pressure on nanoemulsions. This phenomenon could be explained as a better combination of water phase with oil phase in emulsions due to the extension of homogenization time. Thus, seven homogenization cycles were selected as the central point in the following optimization experiments. The fixed variables were homogenization pressure: 60 MPa, emulsifier concentration: 3.0% and oil concentration: 10%.

The effects of emulsifier concentration on particle size and stability of nanoemulsions are shown in Figures 2C and 3C. The particle size of nanoemulsions decreased with increase in the concentration of LYCRPLs with emulsifier concentration in the range of 2.0–4.0%. The particle size reached the lowest value if the LYCRPLs' content was 4.0%, and subsequently increased significantly ($P < 0.05$). This trend may be associated with the higher concentrations of emulsifier, which contribute better surface coverage of particles in nanoemulsions (Pola *et al.*, 2019). Meanwhile, there was no significant difference ($P > 0.05$) in the effect of emulsifier concentration on the stability of emulsion when the emulsifier concentration was 4%. This phenomenon has been reported in another study (Llinares *et al.*, 2018). As mentioned previously, an emulsifier concentration of 4% was selected as the central point. The fixed variables were 60 MPa homogenization pressure, five homogenization cycles, and 10% oil concentration.

As the proportion of oil phase increased gradually, the particle size of nanoemulsions at first decreased but increased subsequently, with gradual increase in the stability of nanoemulsions (Figures 2D and 3D). This phenomenon is explained by the fact that increase in oil concentration reduces the surface tension of emulsion

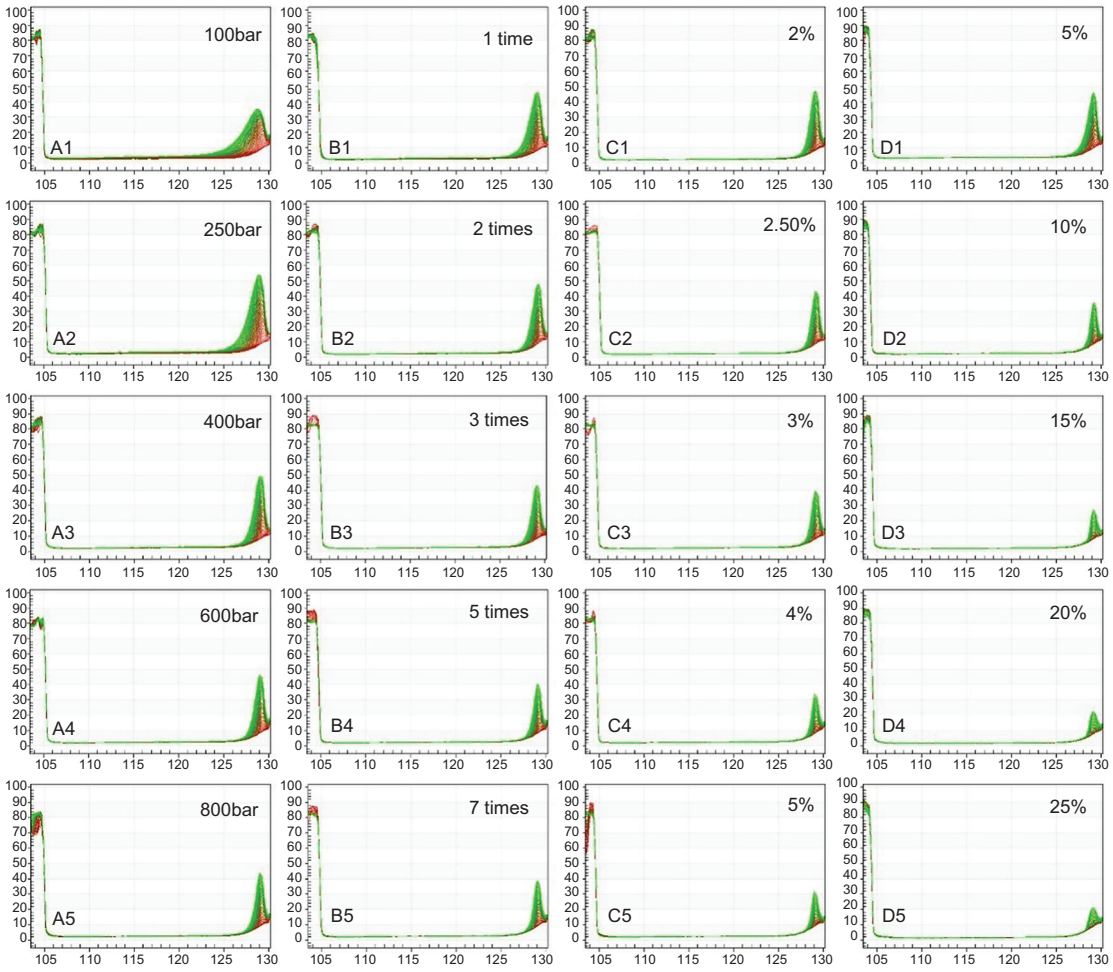


**Figure 3. (A1–A5) Effects of homogenization pressure, (B1–B5) homogenization cycles, (C1–C5) emulsifier concentration, and (D1–D5) oil concentration on the stability of AST nanoemulsions.**

but enhances its stability (Alba *et al.*, 2021). Nevertheless, higher concentration of oil requires more emulsifier. When the proportion of oil phase increases continuously, the fixed emulsifier concentration is not enough to cover the oil droplet surface, which finally increases the particle size of nanoemulsions (Cha *et al.*, 2019). Therefore, an oil concentration of 15% was selected as the central point for further response to surface experiments. The fixed variables were 60 MPa homogenization pressure, five homogenization cycles, and an emulsifier concentration of 3%.

## Fitting the model

The stability, particle size, and PDI values of nanoemulsions obtained from the experiment and their predicted values are given in Table 3. The predicted values agreed well with the data obtained from the response surface design experiment. The experimental data were used to calculate the coefficients of quadratic polynomial equation and to predict the stability, particle size, and PDI values of nanoemulsions.

ANOVA showed that the experimental data could be well expressed by a quadratic polynomial model. The retention coefficients ($R^2$) of emulsion stability ($Y_1$), particle size ($Y_2$) and PDI ($Y_3$) were 0.9561, 0.9768, and 0.9523, respectively (Table 3). The lack of fit was not significant ($P < 0.05$) compared to the pure error of all variables, which indicates that the experimental model is statistically accurate (Gunst, 2008). In this study, $R^2$ is close to unity. This implies that the quadratic polynomial model obtained by using the response surface experimental design was sufficient to describe the influence of the independent variables studied on response variables. This shows that the model fits the experimental findings well. The analysis of variance determines the significant level of quadratic polynomial model coefficients. The smaller *P*-value and larger *F*-value show that the independent variable has a higher significant effect on response variables (Mehmood *et al.*, 2018).

**Table 3.** Predicted and experimental values of nanoemulsion's stability, particle size and polymer dispersity index obtained from the central composite experimental design.

| Std | Run | *P* (MPa) | *C* (cycles) | *E* (%) | *O* (%) | Stability of emulsion | | Particle size (nm) | | PDI | |
|---|---|---|---|---|---|---|---|---|---|---|---|
| | | | | | | Experimental | Predicted | Experimental | Predicted | Experimental | Predicted |
| 1 | 5 | 50 | 6 | 3.5 | 12.5 | 0.102 | 0.099 | 301.10 | 298.12 | 0.412 | 0.358 |
| 2 | 25 | 70 | 6 | 3.5 | 12.5 | 0.064 | 0.060 | 240.50 | 244.74 | 0.273 | 0.276 |
| 3 | 16 | 50 | 8 | 3.5 | 12.5 | 0.072 | 0.078 | 264.60 | 269.29 | 0.438 | 0.478 |
| 4 | 13 | 70 | 8 | 3.5 | 12.5 | 0.058 | 0.051 | 239.40 | 237.74 | 0.514 | 0.443 |
| 5 | 11 | 50 | 6 | 4.5 | 12.5 | 0.102 | 0.102 | 298.00 | 297.43 | 0.569 | 0.543 |
| 6 | 1 | 70 | 6 | 4.5 | 12.5 | 0.057 | 0.054 | 231.30 | 228.27 | 0.413 | 0.421 |
| 7 | 28 | 50 | 8 | 4.5 | 12.5 | 0.100 | 0.095 | 296.60 | 292.27 | 0.654 | 0.639 |
| 8 | 26 | 70 | 8 | 4.5 | 12.5 | 0.054 | 0.060 | 239.90 | 244.94 | 0.512 | 0.564 |
| 9 | 27 | 50 | 6 | 3.5 | 17.5 | 0.087 | 0.080 | 323.50 | 322.58 | 0.907 | 0.866 |
| 10 | 19 | 70 | 6 | 3.5 | 17.5 | 0.066 | 0.069 | 313.90 | 309.92 | 0.951 | 0.957 |
| 11 | 12 | 50 | 8 | 3.5 | 17.5 | 0.041 | 0.042 | 258.70 | 253.42 | 0.628 | 0.611 |
| 12 | 14 | 70 | 8 | 3.5 | 17.5 | 0.045 | 0.045 | 257.90 | 262.59 | 0.712 | 0.749 |
| 13 | 6 | 50 | 6 | 4.5 | 17.5 | 0.057 | 0.062 | 306.60 | 299.95 | 0.476 | 0.538 |
| 14 | 21 | 70 | 6 | 4.5 | 17.5 | 0.049 | 0.042 | 272.10 | 271.53 | 0.618 | 0.588 |
| 15 | 15 | 50 | 8 | 4.5 | 17.5 | 0.035 | 0.039 | 254.60 | 254.48 | 0.251 | 0.259 |
| 16 | 17 | 70 | 8 | 4.5 | 17.5 | 0.032 | 0.033 | 253.20 | 247.87 | 0.311 | 0.356 |
| 17 | 23 | 40 | 7 | 4.0 | 15.0 | 0.094 | 0.092 | 293.50 | 299.49 | 0.523 | 0.546 |
| 18 | 24 | 80 | 7 | 4.0 | 15.0 | 0.041 | 0.046 | 241.30 | 239.50 | 0.586 | 0.562 |
| 19 | 20 | 60 | 5 | 4.0 | 15.0 | 0.060 | 0.067 | 294.00 | 299.14 | 0.373 | 0.410 |
| 20 | 22 | 60 | 9 | 4.0 | 15.0 | 0.041 | 0.036 | 247.60 | 246.65 | 0.338 | 0.299 |
| 21 | 8 | 60 | 7 | 3.0 | 15.0 | 0.059 | 0.063 | 275.30 | 273.80 | 0.720 | 0.769 |
| 22 | 18 | 60 | 7 | 5.0 | 15.0 | 0.055 | 0.054 | 252.70 | 258.39 | 0.611 | 0.561 |
| 23 | 3 | 60 | 7 | 4.0 | 10.0 | 0.094 | 0.097 | 264.40 | 261.60 | 0.405 | 0.438 |
| 24 | 30 | 60 | 7 | 4.0 | 20.0 | 0.051 | 0.050 | 282.00 | 288.99 | 0.773 | 0.739 |
| 25 | 2 | 60 | 7 | 4.0 | 15.0 | 0.055 | 0.053 | 247.30 | 247.50 | 0.388 | 0.354 |
| 26 | 10 | 60 | 7 | 4.0 | 15.0 | 0.048 | 0.053 | 245.00 | 247.50 | 0.308 | 0.354 |
| 27 | 9 | 60 | 7 | 4.0 | 15.0 | 0.052 | 0.053 | 243.60 | 247.50 | 0.373 | 0.354 |
| 28 | 7 | 60 | 7 | 4.0 | 15.0 | 0.054 | 0.053 | 251.70 | 247.50 | 0.413 | 0.354 |
| 29 | 4 | 60 | 7 | 4.0 | 15.0 | 0.057 | 0.053 | 247.70 | 247.50 | 0.356 | 0.354 |
| 30 | 29 | 60 | 7 | 4.0 | 15.0 | 0.049 | 0.053 | 249.70 | 247.50 | 0.284 | 0.354 |

*P*: homogenization pressure; *C*: homogenization cycles; *E*: emulsifier concentration; *O*: oil concentration.

### Effect of independent variables on response variables

Effects of independent variables on nanoemulsion's stability, particle size and PDI are summarized in Table 3. Regression coefficients of independent variables are given in Table 4.

*Stability of Nanoemulsion*

The stability of nanoemulsions was mainly dependent on oil concentration, as it had a significant effect on nanoemulsion's stability at linear ($P < 0.001$), quadratic ($P < 0.001$), and interaction ($P < 0.05$) levels (Table 4). Other factors that contributed significantly to nanoemulsion's stability were the linear terms of homogenization pressure ($P < 0.001$) and homogenization cycles ($P < 0.001$), and quadratic terms ($P < 0.01$) and interaction terms of homogenization pressure ($P < 0.001$) (Table 4).

The interactive effects of emulsifier concentration and oil concentration on nanoemulsion's stability are shown in Figure 4B. Both independent variables exert linear effects on nanoemulsion's stability. Up to a certain level, the stability of nanoemulsions increased with increase in both oil and emulsifier concentrations. This trend was observed since the surface tension of the emulsion can be enhanced with increase in oil concentration (Homayoonfal *et al.*, 2014). The effect of oil concentration is to increase the packing of emulsion droplets, reducing their mobility and hence favoring gravitational separation. These results suggest that both emulsifier and oil concentrations had positive effects on stability. The combined effects of homogenization pressure and oil concentration on the stability of nanoemulsions are shown in Figure 4B, which indicates that homogenization pressure exerts a linear effect while oil concentration had a linear and quadratic effects on the stability of nanoemulsion. There was a downregulation of homogenization pressure and oil concentration with decrease in the stability of nanoemulsion. A possible reason for this decrease is that the smaller droplets were made by higher homogenization pressure. This change can more effectively reduce the rate of gravitational separation, and the droplet velocity increases with the square of diameter (Rao and McClements, 2012).

**Table 4. Regression coefficient values of different responses for preparation of nanoemulsion by using the response surface methodology.**

| Variables[a] | Stability of emulsion | | | Particle size (nm) | | | PDI | | |
|---|---|---|---|---|---|---|---|---|---|
| | Regression coefficient | F-value | P-value | Regression coefficient | F-value | P-value | Regression coefficient | F-value | P-value |
| $a_0$ | 0.053 | | | 247.50 | | | 0.35 | | |
| *Linear* | | | | | | | | | |
| $a_1$ | –0.0115 | 93.01 | <0.0001 | –15.00 | 181.35 | <0.0001 | 0.004 | 0.12 | 0.7328 |
| $a_2$ | –0.0077 | 41.49 | <0.0001 | –13.12 | 138.83 | <0.0001 | –0.028 | 6.00 | 0.0270 |
| $a_3$ | –0.0024 | 3.94 | 0.0658 | –3.85 | 11.98 | 0.0035 | –0.052 | 20.92 | 0.0004 |
| $a_4$ | –0.0118 | 97.09 | <0.0001 | 6.85 | 37.79 | <0.0001 | 0.075 | 43.69 | <0.0001 |
| *Quadric* | | | | | | | | | |
| $a_{11}$ | 0.0041 | 13.24 | 0.0024 | 5.50 | 27.87 | <0.0001 | 0.050 | 22.08 | 0.0003 |
| $a_{22}$ | –0.0002 | 0.03 | 0.8764 | 6.35 | 37.15 | <0.0001 | 0.00026 | 0.0006 | 0.9808 |
| $a_{33}$ | 0.0014 | 1.67 | 0.2154 | 4.65 | 19.92 | 0.0005 | 0.078 | 53.38 | <0.0001 |
| $a_{44}$ | 0.0053 | 22.61 | 0.0003 | 6.95 | 44.50 | <0.0001 | 0.059 | 30.35 | <0.0001 |
| *Interaction* | | | | | | | | | |
| $a_{12}$ | 0.0033 | 5.11 | 0.0391 | 5.46 | 16.01 | 0.0012 | 0.012 | 0.70 | 0.4148 |
| $a_{13}$ | –0.0021 | 1.98 | 0.1798 | -3.94 | 8.36 | 0.0112 | -0.010 | 0.52 | 0.4814 |
| $a_{14}$ | 0.0072 | 24.05 | 0.0002 | 10.18 | 55.73 | <0.0001 | 0.043 | 9.60 | 0.0073 |
| $a_{23}$ | 0.0037 | 6.33 | 0.0237 | 5.92 | 18.83 | 0.0006 | –0.006 | 0.19 | 0.6697 |
| $a_{24}$ | –0.0041 | 7.68 | 0.0142 | –10.08 | 54.64 | <0.0001 | –0.094 | 45.32 | <0.0001 |
| $a_{34}$ | –0.0052 | 12.53 | 0.0030 | –5.48 | 16.15 | 0.0011 | –0.128 | 84.78 | <0.0001 |
| $R^2$ | 0.9561 | | | 0.9768 | | | 0.9523 | | |

Note: [a]$a_0$ is a constant, and $a_i$, $a_{ii}$, and $a_{ij}$ are the linear, quadratic, and interactive coefficients of quadratic polynomial equations, respectively.

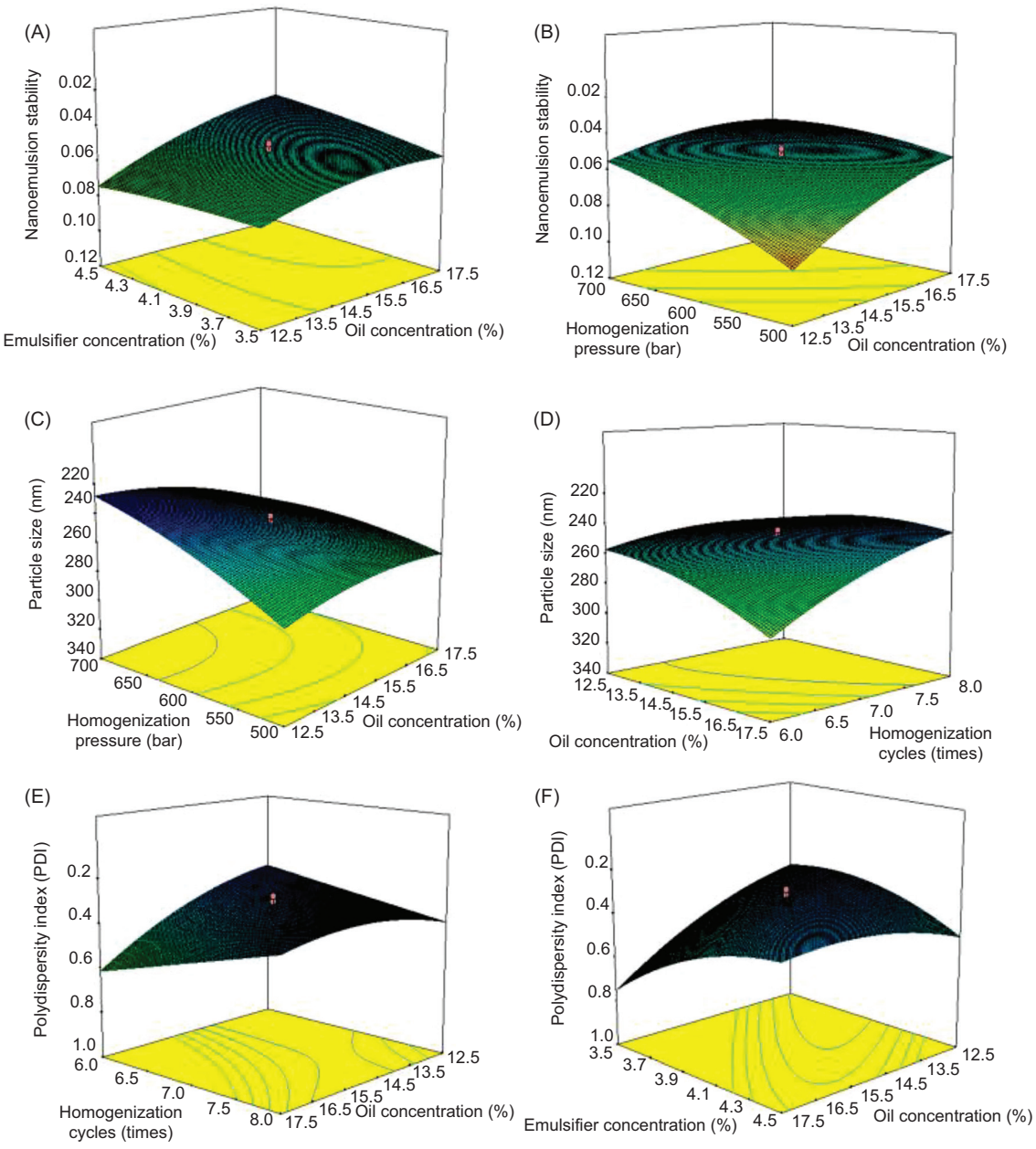


**Figure 4. Response surface plots of (A) nanoemulsions stability versus emulsifier concentration (%) and oil concentration (%); (B) nanoemulsions stability versus homogenization pressure (MPa) and oil concentration (%); (C) particle size (nm) versus homogenization pressure (MPa) and oil concentration (%); (d) particle size (nm) versus oil concentration (%) and homogenization cycles; (E) PDI of nanoemulsions versus homogenization cycles and oil concentration (%); and (F) PDI of nanoemulsions versus emulsifier concentration (%) and oil concentration (%).**

*Particle size*

Considering the particle size, homogenization pressure had a significant effect on the particle size of nanoemulsions at linear ($P < 0.001$), quadratic ($P < 0.001$) and interaction ($P < 0.001$) levels (Table 4). Other factors that significantly contribute to particle size were linear effects of homogenization cycles ($P < 0.001$), emulsifier concentration ($P < 0.01$) and oil concentration ($P < 0.001$); quadratic effects of homogenization cycles ($P < 0.001$), emulsifier concentration ($P < 0.001$) and oil concentration ($P < 0.001$)l and interactive effects of homogenization cycles ($P < 0.001$) and oil concentration ($P < 0.001$) (Table 4).

A contour plot in Figure 4C illustrates the particle size as a function of oil concentration and homogenization

pressure. Both of these independent variables had a linear and quadratic effects on particle size. At lower oil concentration, particle size was reduced with increasing homogenization pressure. This decrease was due to effect of higher homogenization pressure on shear force and other fluid-mechanical stresses, resulting in the reduction of droplet size (Floury *et al.*, 2003). Figure 4D describes the interactive effect of homogenization cycles and oil concentration on particle size, which explained the linear effects of both variables on particle size. Particle size of nanoemulsions reduced with the increased cycles of homogenization. Nonetheless, higher concentration of oil resulted in increase in particle size. Increase of homogenization cycles means extension of homogenization time. This trend was consistent with the previous findings that the particle size decreased with strong shear force (Yuan *et al.*, 2008).

*Polydispersity index*

Polydispersity index is used to measure particle size distribution of emulsion, which evaluates the quality of emulsion (Shi *et al.*, 2021). PDI of nanoemulsions was mainly dependent on oil concentration, which had significant effects on PDI at linear ($P < 0.001$), quadratic ($P < 0.001$) and interaction ($P < 0.01$) levels. Other factors that significantly affected PDI were linear effects of homogenization cycles ($P < 0.05$) and emulsifier concentration ($P < 0.001$); quadratic effects of homogenization pressure ($P < 0.001$) and emulsifier concentration ($P < 0.001$); and interaction effects of homogenization cycles ($P < 0.001$) and emulsifier concentration ($P < 0.001$).

At higher homogenization cycles, a decrease in PDI was observed with increase in oil concentration (as shown in Figure 4e). This decrease in PDI was attributed to strong shear force, which resulted in smaller particle size and higher homogenization cycles, and this way could make both water and oil phase mix thoroughly to form uniform distribution nanoemulsions (Kim *et al.*, 2012). Figure 4F shows the interactive effect of emulsifier and oil concentration on PDI. A decrease in PDI was observed at higher emulsifier and oil concentrations. The reason could be that the emulsifier reduced surface tension in oil–water interface and at the same time improved the bearing capacity of oil phase. This resulted in consistent droplet size of nanoemulsions (Mehmood, 2015).

## Optimization of conditions for preparing nanoemulsions

The optimum conditions for preparing nanoemulsions are as follows: homogenization pressure: 60 MPa; nine homogenization cycles; emulsifier concentration: 4.677%; and oil concentration: 20%. Under these conditions, the predicted values of nanoemulsions' stability, particle size and PDI are 0.013, 252.3 nm and 0.170, respectively.

## Verification of results

Considering the feasibility of practical operation, the above-mentioned processing conditions were applied in three experiments with some modifications: homogenization pressure: 60 MPa; nine homogenization cycles; emulsifier concentration: 4.7%; and oil concentration: 20%. Under the optimum conditions, the experimental values of nanoemulsions' stability, particle size and PDI were 0.018 ± 0.0016, 247 ± 4.5 nm and 0.215 ± 0.019, respectively. The result revealed that the model was satisfactory and accurate.

## Characterization of AST nanoemulsions

Characterization was measured under the optimal preparing conditions of AST nanoemulsions. Figure 5A displays the particle size distribution of nanoemulsions. The PDI value described that AST nanoemulsions had a narrow particle size distribution (Ma and Mu, 2016). Figure 5B shows the TEM observation of the droplets of AST nanoemulsions, and it was observed that nanoemulsion droplets were more or less spherical in shape and nonaggregated, which was consistent with the findings of a previous study (Li *et al.*, 2017).

## Storage stability of AST nanoemulsions

During food processing, storage temperature and time are crucial factors for evaluating quality of nanoemulsions; hence, we monitored the particle size, PDI and zeta-potential values of nanoemulsions at scheduled time intervals during 4-week storage period to evaluate their storage stability. As depicted in Figures 6A and 6B, regardless of temperature, the particle size and PDI of nanoemulsions showed an increasing trend. It is considered that this phenomenon is related to the ripening of Ostwald (Reyes *et al.*, 2021). With the extension of storage period, the quality of emulsion changed gradually, with continuous increase in particle size (Young and Nitin, 2019). In general, the system is considered to be relatively stable when the zeta-potential reaches 25 mV in absolute value (Chen *et al.*, 2020). Figure 6C demonstrates that the zeta-potential values increased with the increase of storage days, and the absolute value was above 25 mV at 5°C and 25°C during storage days, which depicted that AST nanoemulsions prepared by LYCRPLs could be stable for 28 days at 5°C and 25°C, and became slightly unstable at higher temperature. This result was inconsistent with particle size and PDI.

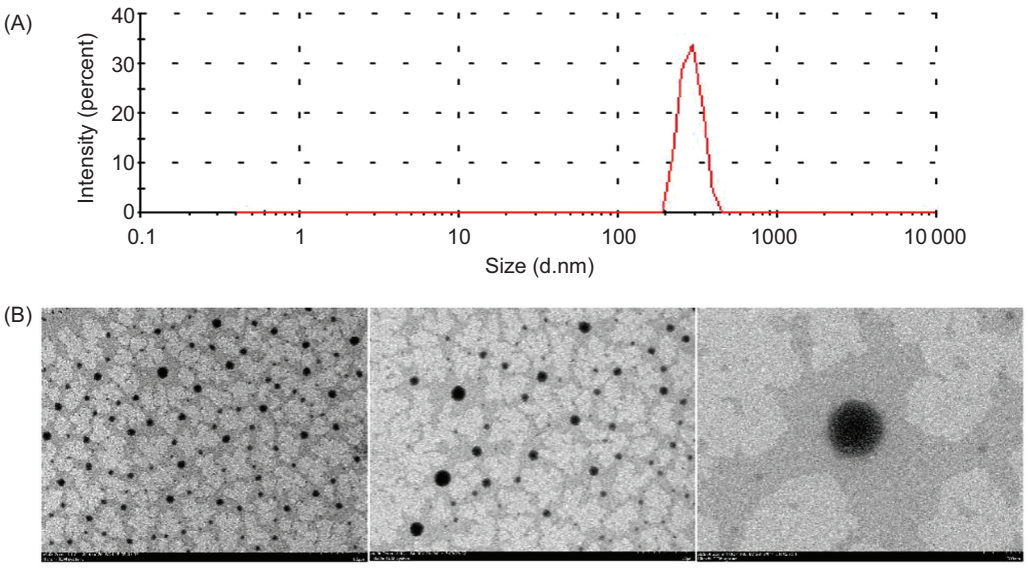


**Figure 5. (A) Particle size distribution of AST nanoemulsions with optimal preparing conditions. (B) Transmission electron microscope (TEM) observations of droplets of AST nanoemulsions under optimal preparing conditions.**

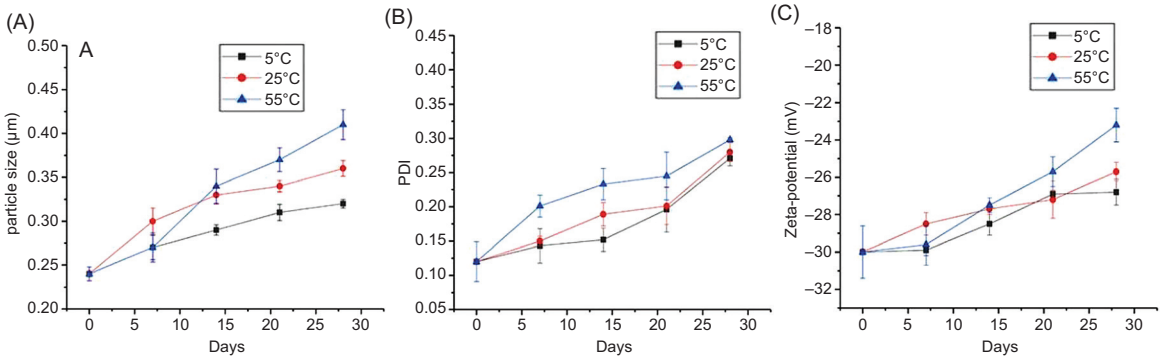


**Figure 6. Changes in (A) particle size, (B) PDI and (C) zeta-potential value of AST nanoemulsions during storage.**

## Conclusion

In this study, AST nanoemulsions were prepared using LYCRPLs as an emulsifier. The four parameters of homogenization pressure, homogenization cycles, emulsifier concentration, and oil concentration for AST nanoemulsions prepared by LYCRPLs were optimized systematically, and droplets of nanoemulsions were characterized by TEM. LYCRPLs have good emulsifying capacity, which could be used as a potential emulsifier. Therefore, differences in the emulsifying properties of LYCRPLs and traditional commercial lecithin need further research.

## Acknowledgments

This research was supported by the National Natural Science Foundation of China (31801465). It was also supported by the Outstanding Young Scientific Research Project of Fujian Agriculture and Forestry University (xjq 201808).

## Author Contribution

Peng Liang provided the idea of this study and interpreted the results. Luyao Huang designed the study and drafted the manuscript. Lingyun Zhang collected test data, and Ruifen Li helped to revise the manuscript.

## Conflict of Interest

The authors declare that they have no conflicts of interest concerning this article. There was no financial support, except those mentioned in the acknowledgments.

## References

Ambati, R.R., Phang, S.M., Ravi, S and Aswathanarayana, R.G. 2014. Astaxanthin: sources, extraction, stcapacity, biological activities and its commercial applications—a review. Marine Drugs. 12(1):128–152. https://doi.org/10.3390/md12010128

Alba, K., Dimopoulou, M. and Kontogiorgos, V. 2021. Baobab polysaccharides as emulsifiers. LWT-Food Sci Technol. 144:111235. https://doi.org/10.1016/j.lwt.2021.111235

Cha, Y., Shi, X.J., Wu, F., Zou, H.N., Chang, C.T., Guo, Y.N., et al. 2019. Improving the stability of oil-in-water emulsions by using mussel myofibrillar proteins and lecithin as emulsifiers and high-pressure homogenization. J Food Eng. 258:1–8. https://doi.org/10.1016/j.jfoodeng.2019.04.009

Chen, Y., Ge, H., Zheng, Y., Zhang, H., Li, Y., Su, X.R., et al. 2020. Phospholipid–protein structured membrane for microencapsulation of DHA oil and evaluation of its in vitro digestibility: inspired by milk fat globule membrane. J Agricul Food Chem. 68(22):6190–6201. https://doi.org/10.1021/acs.jafc.0c01250

Donsì, F., Wang, Y. and Huang, Q. 2011. Freeze–thaw stability of lecithin and modified starch-based nanoemulsions. Food Hydrocoll. 25(5):1327–1336. https://doi.org/10.1016/j.foodhyd.2010.12.008

Dickinson, E. 2009. Hydrocolloids as emulsifiers and emulsion stabilizers. Food Hydrocoll. 23(6):1473–1482. https://doi.org/10.1016/j.foodhyd.2008.08.005

Floury, J., Desrumaux, A., Axelos, M.A.V. and Legrand, J. 2003. Effect of high pressure homogenisation on methylcellulose as food emulsifier. J Food Eng. 58(3):227–238. https://doi.org/10.1016/S0260-8774(02)00372-2

Gunst, R.F. 2008. Response surface methodology: process and product optimization using designed experiments. Technometrics. 38(3):284–286. https://doi.org/10.1080/00401706.1996.10484509

Homayoonfal, M., Khodaiyan, F. and Mousavi, S.M. 2014. Walnut oil nanoemulsion: optimization of the emulsion capacity, cloudiness, density, and surface tension. J Dispers Sci Technol. 35(5):725–733. https://doi.org/10.1080/01932691.2013.807742

Hui, G., Liu, W., Feng, H., Li, J., and Gao, Y. 2016. Effects of chitosan combined with nisin treatment on storage quality of large yellow croaker (*Pseudosciaena crocea*). Food Chem. 203:276–282. https://doi.org/10.1016/j.foodchem.2016.01.122

Ju, H.P., Yeo, I.J., Ji, H.H., Suh, J.W., Lee, H.P. and Jin, T.H. 2017. Anti-inflammatory effect of astaxanthin in phthalic anhydride-induced atopic dermatitis animal model. Exp Dermatol. 27(4):378–385. https://doi.org/10.1111/exd.13437

Komaiko, J., Sastrosubroto, A. and McClements, D.J. 2016. Encapsulation of ω-3 fatty acids in nanoemulsion-based delivery systems fabricated from natural emulsifiers: sunflower phospholipids. Food Chem. 203:331–339. https://doi.org/10.1016/j.foodchem.2016.02.080

Kralova, I. and Sjöblom, J. 2009. Surfactants used in food industry: a review. J Dispers Sci Technol. 30(9):1363–1383. https://doi.org/10.1080/01932690902735561

Kim, D.M., Hyun, S.S., Yun, P., Lee, C.H. and Byun, S.Y. 2012. Identification of an emulsifier and conditions for preparing stable nanoemulsions containing the antioxidant astaxanthin. Int J Cosmet Sci. 34(1):64–73. https://doi.org/10.1111/j.1468-2494.2011.00682.x

Kim W., Wang Y. and Selomulya C. 2020. Dairy and plant proteins as natural food emulsifiers. Trends Food Sci Technol. 105:261–272. https://doi.org/10.1016/j.tifs.2020.09.012

Li, Z., Dong, X., Liu, H., Chen, X., Shi, H., Fan, Y., et al. 2012. Astaxanthin protects ARPE-19 cells from oxidative stress via upregulation of Nrf2-regulated phase II enzymes through activation of PI3K/Akt. Mol Vision. 19(4):1656–1666.

Li, X., Wang, L. and Wang, B. 2017. Optimization of encapsulation efficiency and average particle size of *Hohenbuehelia serotina* polysaccharides nanoemulsions using response surface methodology. Food Chem. 229:479–486. https://doi.org/10.1016/j.foodchem.2017.02.051

Liang, P., Li, R., Sun, H., Zhang, M., Cheng, W., Chen, L., et al. 2018. Phospholipids composition and molecular species of large yellow croaker (*Pseudosciaena crocea*) roe. Food Chem. 245:806–811. https://doi.org/10.1016/j.foodchem.2017.11.108

Liu, C., Tan, Y., Xu, Y., McCleiments, D.J. and Wang, D. 2019. Formation, characterization, and application of chitosan/pectin-stabilized multilayer emulsions as astaxanthin delivery systems. Int J Biological Macromol. 140:985–997. https://doi.org/10.1016/j.ijbiomac.2019.08.071

Llinares, R., Santos, J., Trujillo-Cayado, L.A., Ramírez, P. and Muñoz, J. 2018. Enhancing rosemary oil-in-water microfluidized nanoemulsion properties through formulation optimization by response surface methodology. LWT – Food Sci Technol. 97:370–375. https://doi.org/10.1016/j.lwt.2018.07.033

Ma, M.M. and Mu, T.H. 2016. Effects of extraction methods and particle size distribution on the structural, physicochemical, and functional properties of dietary fiber from deoiled cumin. Food Chem. 194:237–246. https://doi.org/10.1016/j.foodchem.2015.07.095

Martínez-delgado, A.A., Khandual, S. and Villanueva-Rodríguez, S.J. 2017. Chemical stability of astaxanthin integrated into a food matrix: effects of food processing and methods for preservation. Food Chem. 225:23–30. https://doi.org/10.1016/j.foodchem.2016.11.092

McClements, D.J. and Gumus, C.E. 2016. Natural emulsifiers – biosurfactants, phospholipids, biopolymers, and colloidal particles: molecular and physicochemical basis of functional performance. Adv Coll Interface Sci. 234:3–26. https://doi.org/10.1016/j.cis.2016.03.002

Mehmood, T. 2015. Optimization of the canola oil based vitamin E nanoemulsions stabilized by food grade mixed surfactants using response surface methodology. Food Chem. 183:1–7. https://doi.org/10.1016/j.foodchem.2015.03.021

Mehmood, T., Ahmed, A., Ahmad, A., Ahmad, M.S. and Sandhu, M.A. 2018. Optimization of mixed surfactants-based β-carotene nanoemulsions using response surface methodology: an ultrasonic homogenization approach. Food Chem. 253:179–184. https://doi.org/10.1016/j.foodchem.2018.01.136

Nagendraprabhu, P. and Sudhandiran, G. 2011. Astaxanthin inhibits tumor invasion by decreasing extracellular matrix production and induces apoptosis in experimental rat colon carcinogenesis by modulating the expressions of ERK-2, NFkB and COX-2. Invest New Drugs. 29(2):207–224. https://doi.org/10.1007/s10637-009-9342-5

Pan-Utai W., Boonpok S. and Pornpukdeewattana S. 2021. Combination of mechanical and chemical extraction of astaxanthin from *Haematococcus pluvialis* and its properties of microencapsulation. Biocatal Agric Biotechnol. 33:101979. https://doi.org/10.1016/j.bcab.2021.101979

Pogorzelska, E., Godziszewska, J., Brodowska, M. and Wierzbicka, A. 2017. Antioxidant potential of *Haematococcus pluvialis* extract rich in astaxanthin on colour and oxidative stcapacity of raw ground pork meat during refrigerated storage. Meat Sci. 135:54–61. https://doi.org/10.1016/j.meatsci.2017.09.002

Pola, C.C., Moraes, A.R.F., Medeiros, E.A.A., Teófilo, R.F., Soares, N.F.F. and Gomes, C.L. 2019. Development and optimization of pH-responsive PLGA-chitosan nanoparticles for triggered release of antimicrobials. Food Chem. 295:671–679. https://doi.org/10.1016/j.foodchem.2019.05.165

Rao, J.J. and McClements, D.J. 2012. Lemon oil solubilization in mixed surfactant solutions: rationalizing microemulsion & nanoemulsion formation. Food Hydrocoll. 26(1):268–276. https://doi.org/10.1016/j.foodhyd.2011.06.002

Reyes, Y., Hamzehlou, S. and Leiza, J.R. 2021. Ostwald ripening in nano/miniemulsions in the presence of two costabilizers as revealed by molecular dynamics simulations. J Mol Liquids, 335:116152. https://doi.org/10.1016/j.molliq.2021.116152

Shu, G., Khalid, N., Chen, Z., Neves, M.A., Barrow, C.J. and Nakajima, M. 2018. Formulation and characterization of astaxanthin-enriched nanoemulsions stabilized using ginseng saponins as natural emulsifiers. Food Chem. 255:67–74. https://doi.org/10.1016/j.foodchem.2018.02.062

Shi, Y., Wang, W., Zhu, X., Wang, B., Hao, Y., Wang, L. and Elfalleh, W. 2021. Preparation and physicochemical stability of hemp seed oil liposomes. Indust Crops Prod. 162:113283. https://doi.org/10.1016/j.indcrop.2021.113283

Xi, Y., Nisar, T., Hou, Y., Gou, XJ., Sun, L. and Guo, Y. 2018. Pomegranate peel pectin can be used as an effective emulsifier. Food Hydrocoll. 85:30–38. https://doi.org/10.1016/j.foodhyd.2018.06.042

Young, S. and Nitin, N. 2019. Thermal and oxidative stability of curcumin encapsulated in yeast microcarriers. Food Chem. 275:1–7. https://doi.org/10.1016/j.foodchem.2018.08.121

Yuan, Y., Gao, Y., Mao, L. and Zhao, J. 2008. Optimisation of conditions for the preparation of β-carotene nanoemulsions using response surface methodology. Food Chem. 107(3):1300–1306. https://doi.org/10.1016/j.foodchem.2007.09.015